Propagation Characteristics of Wideband MIMO Channel in Urban Micro- and Macrocells

(Invited Paper)

Jianhua Zhang*, Di Dong*, Yanping Liang*, Xin Nie*, Xinying Gao*, Yu Zhang*, Chen Huang* and Guangyi Liu†
* Beijing University of Posts and Telecommunications, Beijing, China, 100876
Email: jhzhang@bupt.edu.cn, {dongdi, liangyanping, niexin, gaoxinying, zhangyu, huangchen}@mail.wtilabs.cn
† Research Institute of China Mobile, Beijing, China, 100053
Email: liuguangyi@chinamobile.com

***Abstract*—The wideband channel measurements at 580 MHz, 2.35 GHz and 4.90 GHz have been performed in the urban micro- and macrocell scenarios in the cities of China with multiple-input multiple-output (MIMO) channel sounder. The measured cases include line-of-sight (LOS) and non-line-of-sight (NLOS) propagation. Statistical results and comparative analysis for both scenarios are presented in this paper, including path loss (PL), root mean square (rms) delay spread (DS) and maximum excess delay (maxED), and angular spread (AS). In NLOS case, the frequency dependent factor (FDF) is observed as 32.1 by fitting the PL model of 2.35 GHz and 4.90 GHz. Moreover, a larger rms DS in urban microcell and AS at both base station (BS) and mobile subscriber (MS) are found for the denser and higher buildings in the cities of China. As the frequency varying from 580 MHz to 4.90 GHz, the median rms DS is decreased from 330 ns to 130 ns for NLOS case.**

I. Introduction

Compared to IMT-2000, the propagation characteristics and models of IMT-Advanced system are needed due to the disconnected carrier frequencies, extended bandwidth and emerging new techniques [1], [2]. The large scale fading effects are important for coverage prediction and interference analysis of IMT-Advanced system [3]. Thus path loss (PL) and shadow fading should be investigated from UHF 450MHz to 3.60GHz allocated at WRC07 for IMT-Advanced system. Secondly, the bandwidth from 20MHz to 100MHz is required in order to support the high data rate service from 20Mbps to 1Gbps. So the delay spread (DS) characteristic of wideband channel is significant to reveal the coherence bandwidth and frequency selectivity of channel [4]. Finally, multiple-input and multiple-output (MIMO) is one of the most promising techniques for IMT-Advanced system [5], [6]. It is verified that the angular spread (AS) of each cluster and composite AS affects both ergodic and outage capacity greatly [7]. Thus the properties of AS at both the transmitter (Tx) and the receiver (Rx) should be exactly modeled to validate the MIMO schemes. So wideband MIMO channel measurement and models have attracted a lot of research interests for its crucial impact on the system design, evaluation and deployment of IMT-Advanced system [8]–[13].

In urban scenarios, the propagation characteristics are influenced by the density, height and distribution of buildings, etc.

(a) East view (b) West view

Fig. 1. One of measurement environments in Shijiazhuang

Wireless World Initiative New Radio (WINNER) project has implemented a series of measurement campaigns in European and North American cities, channel characteristics of which have been summarized in [8]. Compared to Europe, Asia cities like Beijing (BJ) have the higher building density and height in order to satisfy the demands of the high population. One example of our measured urban environments is shown in Fig. 1 and the compact high buildings could be observed viewing from base station (BS) to east and west directions. So in order to investigate the propagation characteristics of IMT-Advanced carrier frequencies in the cities of China, we conducted the wideband MIMO channel measurements in both urban micro- and macrocells.

In this paper, PL is modeled in the log-distance expression based on the measured channel impulse responses (CIRs). The empirical cumulative distribution functions (CDFs) of the root mean square (rms) DS and the median maximum excess delay (maxED) are statistically summarized. Moreover, the Spatial-Alternating Generalized Expectation-maximization (SAGE) [14] algorithm is utilized to extract the double-directional spatial parameters from measured CIRs. Then AS of BS and mobile subscriber (MS) is presented based on the estimated results from SAGE. The rest of the paper is organized as follows. In Section II, the measurement system and environments are described. In Section III, the channel characteristics are presented from three perspectives, i.e. PL, DS and AS. Finally, the conclusions are drawn in Section IV.

978-1-4244-2644-7/08/$25.00 ©2008 IEEE

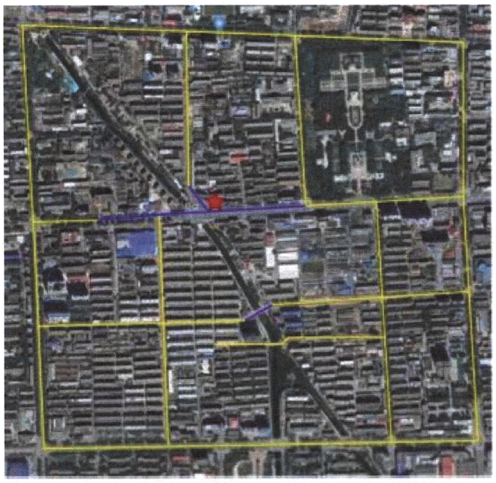

(a) Shijiazhuang

(b) Beijing

Fig. 2. Measured routes in the urban environments

II. Channel Measurement Campaigns

Extensive measurements of urban micro- and macrocells were performed in winter in two cities respectively, Shijiazhuang (SJZ) and BJ. We chose SJZ for its compact grid building layout, which is similar to the Manhattan structure used in IMT-2000 urban microcell scenario (Fig. 2(a)). The well developed BJ is selected because it has the increasing demand for mobile services. Thus its propagation characteristics are important for the future deployment of IMT-Advanced system (Fig. 2(b)). Compared Fig. 2(b) with Fig. 2(a), the irregular building layout of BJ is less dense than that of SJZ. So the measured site of BJ is designed for urban macrocell scenario.

TABLE I
THE MEASUREMENT SITE INFORMATION

Scenario	City	Average building height	BS/MS antenna height	Average building density
Urban microcell	Shijiazhuang (micro-SJZ)	25m	24m/3.1m	34%
Urban macro-cell	Beijing (macro-BJ)	20m	28m/2.6m	20%
	Shijiazhuang (macro-SJZ)	25m	30m/2.6m	34%

Table I lists the measured site information for both scenarios. In urban micro-SJZ, the antenna of BS is installed at the top of a 7-floor building and it is a bit lower than the average building height. In urban macro-SJZ, the antenna of BS is set on a commercial BS of 30m and it is fixed on the rooftop of an 8-floor building in urban macro-BJ. The maximum distance between BS and MS is about 1000m and the average speed of MS was 8m/s and 10m/s for microcell and macrocell, respectively. In Fig. 2, the yellow, blue and red lines are specified as the routes in non-line-of-sight (NLOS), line-of-sight (LOS) and obstructed-line-of-sight (OLOS) propagation correspondingly. The star mark denotes the location of BS antenna. The antenna of MS is installed at the top of a van during measurements.

Measured MIMO data were recorded with Elektrobit PropSound channel sounder [15], which uses the periodic pseudo-random binary signals and time-domain multiplexed switching of Tx and Rx antennas. During the measurements, mobile routes of MS were recorded using the Global Positioning System (GPS).

The detail parameters of channel sounder are given in Table II. MS employs a 3D dual-polarized Omni-Directional Array (ODA) with maximum 56 elements shown in Fig. 3(a); BS employs a dual-polarized Uniform Planar Array (UPA) shown in Fig. 3(b) at 2.35GHz measurements. The element spacing of both ODA and UPA is half of a wavelength, $\lambda/2$. In our measurements, BS antenna only uses 8 elements of UPA and 32 or 16 elements of ODA are chosen for MS antenna. For ease of comparison about the channel characteristics of different carrier frequencies, Vertical-polarized Dipole Antenna (VDA) is used in macro-SJZ measurement.

III. Propagation Characteristics

After measurement, post processing is implemented and it consists of two procedures: 1) obtaining CIR from raw data; 2) extracting channel parameters, such as delay, power and angles, etc. In this section, PL, rms DS and maxED, and AS statistics are analyzed for urban micro- and macrocell scenarios.

In order to satisfy the wide-sense stationary and uncorrelated scattering (WSSUS) condition, the raw CIRs should be divided into sub-sets, and averaged according to

$$h_{\text{av}}(\tau) = E_t\{h(t,\tau)\} \tag{1}$$

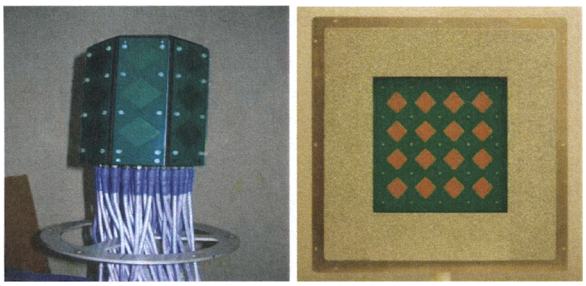

(a) ODA (b) UPA

Fig. 3. Antenna arrays used in measurements

TABLE II
SOUNDER PARAMETERS IN MEASUREMENTS

Scenarios	Microcell	Macrocell		
Carrier freq. [MHz]	2350	580	2350	4900
Bandwidth [MHz]	100	25	100	100
Chip rate [MHz]	200	50	200	200
Code length [chips]	1023	1023	1023	1023
Tx power [dBm]	33	33	40	40
Cycle rate [Hz]	160.2	21.2	436.4	614.8
Antenna at BS	UPA	UPA	UPA/VDA	UPA/VDA
Antenna at MS	ODA	VDA	ODA	ODA
# of channels (BS×MS)	32×8	SJZ:16×1	BJ:16×8 SJZ:1×50	BJ:16×8 SJZ:1×50

where $E_t\{\cdot\}$ denotes the average in time domain. In the mobile measurements, the time span for averaging corresponds to a suitable window length around 20λ [10]. To separate the noise from the measured multipath components (MPCs), the dynamic range is set as 20 dB from the strongest path for both LOS and NLOS cases.

A. PL models

After noise cutting and MPCs search, the measured PL values are calculated in dB as:

$$PL = -10\log_{10}\left(\sum_{\tau}|h_{\text{av}}(\tau)|^2\right) + G_{\text{Tx}} + G_{\text{Rx}} \quad (2)$$

where G_{Tx} and G_{Rx} denotes the gains of the underlying Tx and Rx antenna respectively. The values of G_{Tx} and G_{Rx} can be calculated from the antenna response. To extract the large-scale characteristics, a linear curve fitting method is used which fits the decibel path loss to the decibel distance with a random variation. The empirical model of log-distance PL described in [16] is written as

$$PL(d) = PL_0 + 10n \cdot \log_{10} d + X_\sigma \quad (3)$$

where PL_0 represents the intercept, d is the separation distance of Tx-Rx expressed in meters, and n denotes the PL exponent which indicates the rate at which PL increases with respect to distance. The value of n is dependent on the specific propagation environment, like building density and height, etc.

TABLE III
THE FITTED PL INTERCEPT, EXPONENT AND STANDARD DEVIATION

		Microcell	Macrocell		
		2.35GHz (SJZ)	2.35GHz (BJ)	2.35GHz (SJZ)	4.90GHz (SJZ)
LOS	PL_0	45.6	42.6	32.5	36.2
	n	2.2	2.1	2.4	2.5
	σ	2.4	2.6	1.9	3.7
NLOS	PL_0	12.4	44.4	10.6	29.1
	n	3.7	3.1	3.6	3.2
	σ	4.8	2.8	5.5	5.0

Considering the fact that with the same Tx-Rx distance, the surroundings of the Tx and the Rx in one scenario might be vastly different from those in another scenario, the log-normal shadow fading is modeled by a zero-mean Gaussian random variable X_σ in (3) with standard deviation σ. The values of PL_0 and n are identified by using the least square (LS) method, i.e. the difference between the measured and estimated PL is minimized in a mean square error sense over a wide range of measurement locations. For comparison purpose, the PL model in the scenario of free space propagation

$$PL_{\text{FS}}(d) = 20\log_{10}\left(\frac{4\pi d}{\lambda}\right) \quad (4)$$

given by Friis equation [17] is considered. The antenna gains are excluded. This model is used to predict the received signal strength when the Tx and Rx have a clear, unobstructed LOS path between them. In this case, the PL exponent n is equal to 2.

Hata model applicable from 150MHz to 1500MHz [18] and COST-231 Hata model enhanced to 2.0GHz [19] have been provided based on the urban measurements. They are widely used in the research and deployment of terrestrial mobile systems from UHF band to 2.0GHz. So in Table III we mainly summarize our fitted PL models above 2.0GHz for urban micro- and macrocells. In LOS case, the unobstructed propagation brings to all of exponent n are similar and a bit larger than 2 of the free space. Compared with the results of 2.35GHz, macro-SJZ at 4.90GHz has the slightly larger PL exponent and standard deviation in this case. As for NLOS case, the exponent n of micro-SJZ is 3.7 and is a bit larger than those of macro-BJ and macro-SJZ. The reason is that the antenna of microcell is lower than the average building height and this leads to more obstructions and fading than that of macrocell. Compared SJZ with BJ, the standard deviation in SJZ is higher than that of BJ since the selected site of SJZ has the denser buildings than BJ.

To explore the relation between the carrier frequency and PL, a frequency dependent factor (FDF) C is introduced to (3), and then PL model is expressed as [8]

$$PL(d) = PL_0 + 10n \cdot \log_{10} d + X_\sigma + C \cdot \log_{10}\left(\frac{f_c}{f_0}\right) \quad (5)$$

where f_0 is the reference frequency and f_c is the system frequency. Similarly LS method is used to extract the values

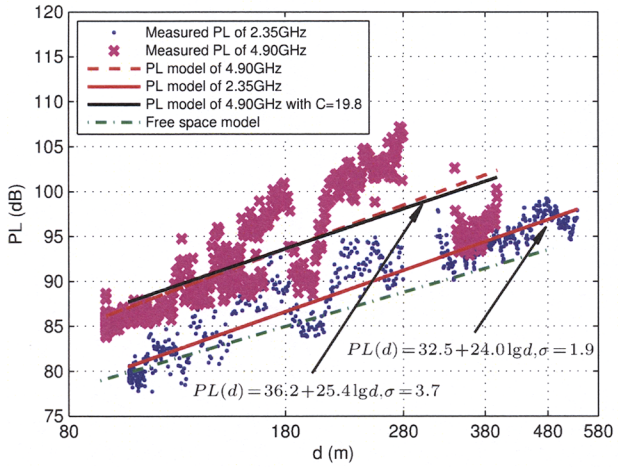

Fig. 4. PL models for macro-SJZ LOS at 2.35GHz and 4.90 GHz

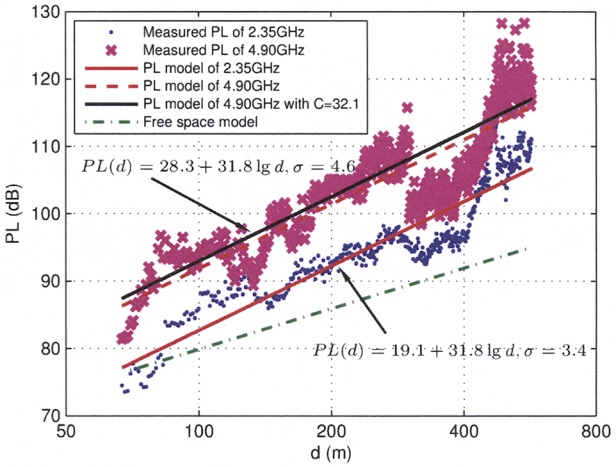

Fig. 5. PL models for macro-SJZ NLOS at 2.35GHz and 4.90 GHz

of PL_0, n and C with the measured data of the different frequencies. Considering the relation that $\lambda = \frac{c}{f_c}$ and c is the constant of speed light, the free space PL is changed to

$$PL_{\text{FS}}(d) = 20\log_{10} f_c + 20\log_{10}\left(\frac{4\pi d}{\lambda}\right) \tag{6}$$

Thus the FDF C is equal to 20 in free space case.

In Fig. 4, PL models of urban macro-BJ LOS at 2.35GHz and 4.90GHz are plotted within break point distance. It can be observed that PL models of 4.90GHz and 2.35GHz are nearly two parallel lines. Using (5) and assuming $f_0 = 2.35$GHz , the FDF C is equal to 19.8, which is very close to 20 in free space. WINNER also gives FDF as 20 from 2.0GHz to 6.0GHz within break point distance [8]. It's reasonable that in LOS case, the propagation characteristic is very close to free space. However, for NLOS case in Fig. 5, the fitted FDF as 32.1 with $f_0 = 2.35$GHz is much larger than 23 given in WINNER [8], such that the higher carrier frequency brings more loss at NLOS case in the cities of China and the future system at the higher carrier frequency requires more transmit power to cover the same areas as the lower carrier frequency.

B. Delay spread

MaxED and rms could be calculated directly from the power delay profile of each measured snapshot. MaxED is written as τ_{max} and it is the delay difference between the first and the last MPC above the dynamic range threshold. The rms DS is calculated as the standard deviation of the excess delays weighted with the power and given, i.e.

$$\tau_{\text{rms}} = \sqrt{\left(\sum_{\ell=1}^{L} P_\ell\right)^{-1} \sum_{\ell=1}^{L} P_\ell \tau_\ell^2 - \left(\sum_{\ell=1}^{L} P_\ell\right)^{-2} \left(\sum_{\ell=1}^{L} P_\ell \tau_\ell\right)^2} \tag{7}$$

where τ_ℓ and P_ℓ denote respectively, the excess delay and power of the lth path. The CDF of rms DS is well fitted by log-normal distribution as

$$\tau_{\text{rms}} = 10^{\mu_{\text{DS}} + X_{\sigma_{\text{DS}}}} \tag{8}$$

where X is a zero-mean Gaussian random variable with a unit variance. $\mu_{\text{DS}} = E\{\log_{10}\tau_{\text{rms}}\}$ and $\sigma_{\text{DS}}^2 = \text{Var}\{\log_{10}\tau_{\text{rms}}\}$ are the logarithmic mean and standard deviation of the DS respectively.

Using the measurement equipment with 10MHz and 5MHz chip rate, 300ns-500ns rms DS has been observed [3], [20]. It has been analyzed that narrow bandwidth measurement leads to the larger DS in [4]. In Table IV, our results of maxED and rms DS for both urban microcell and macrocell with 2.35GHz and 100MHz bandwidth are listed. The same wideband measurement results from WINNER for 2.0GHz to 6.0GHz [8] are fairly compared in Table IV. It can be observed that in LOS case, we have the similar mean rms DS as WINNER's in both urban microcell and macrocell. However, In NLOS case, a large mean rms DS is obtained in urban microcell as 158ns and it is two times of WINNER's result, which means the channels in China are more frequency selective. It comes from that the dense and grid distributed buildings make more reflected and scattered paths appearing in urban microcell scenario. Such environment characteristic leads to that the larger standard variance of rms DS in all cases is observed.

In Fig. 6, the empirical CDF curves of the rms DS are plotted for 580MHz, 2.35GHz and 4.90GHz in urban macro-SJZ scenario. As the frequency varying from 580MHz to 4.90GHz, the median rms DS is decreased from 110ns to 40ns for LOS case and from 330ns to 130ns for NLOS case. The same tendency varying from 700ns to 270ns has been concluded as from 430MHz to 5750MHz with 10MHz measurement bandwidth [20]. A reasonable explanation is that for the higher carrier frequency, the paths with the larger delay undergo more rounds of reflection and longer propagation distance, then arrive with poor power, even below the noise level. Those

TABLE IV
COMPARISON OF THE STATISTICAL DELAY CHARACTERISTIC PARAMETERS

Scenarios		Urban microcell		Urban macrocell	
		2.35GHz (SJZ)	WINNER [8]	2.35GHz (BJ)	WINNER [8]
LOS	50% τ_{max} [ns]	435	N/A	310	N/A
	50% τ_{rms} [ns]	73	N/A	49	N/A
	μ_{DS} [$\log_{10}$(s)]	−7.23	−7.44	−7.37	−7.39
	σ_{DS} [$\log_{10}$(s)]	0.52	0.25	0.69	0.63
NLOS	50% τ_{max} [ns]	960	N/A	1600	N/A
	50% τ_{rms} [ns]	164	N/A	251	N/A
	μ_{DS} [$\log_{10}$(s)]	−6.80	−7.12	−6.68	−6.63
	σ_{DS} [$\log_{10}$(s)]	0.43	0.12	0.39	0.32

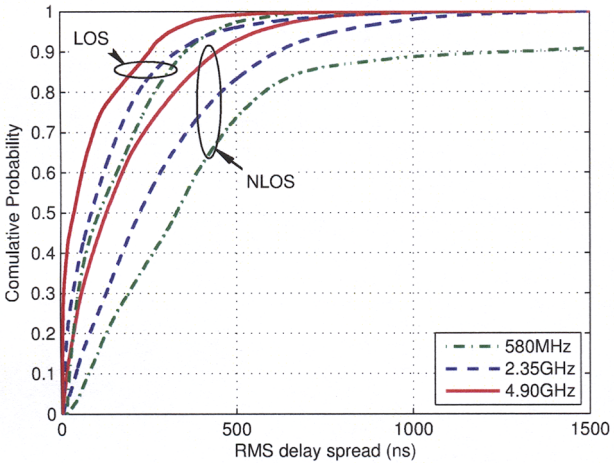

Fig. 6. The empirical CDFs of rms DS in urban macro-SJZ at 580 MHz, 2.35 GHz and 4.90 GHz

paths are ignored after noise cutting. Consequently, the rms DS decreases.

C. Angular spread of AOD and AOA

To evaluate the azimuth spread characteristics at BS and MS numerically, the rms AS is calculated as the root second central moment of power angular spectrum. To avoid the ambiguous effect due to the circular wrapping of the angles, the circular AS (CAS) is calculated. This AS is constant regardless of the value of the angle shift as in the case described in 3GPP spatial channel model (SCM) specification [15]. The CAS is calculated by following steps.

Let $\psi_\ell(\Delta) = \psi_\ell + \Delta$ represent the shifted angle with Δ denoting certain angular shift, the corresponding rms AS ψ_{rms} of $\psi_\ell(\Delta)$ is computed via the minimum operation

$$\begin{aligned}\psi_{\text{rms}} &= \arg\min_{\Delta} \psi_{\text{rms}}(\Delta) \\ &= \arg\min_{\Delta}\left\{\left(\sum_{\ell=1}^{L} P_\ell\right)^{-1}\sum_{\ell=1}^{L}[\psi_\ell(\Delta)-\beta(\Delta)]^2 P_\ell\right\}^{\frac{1}{2}}\end{aligned} \tag{9}$$

where $\beta(\Delta)$ is defined as

$$\beta(\Delta) = \left(\sum_{\ell=1}^{L} P_\ell\right)^{-1}\sum_{\ell=1}^{L}\psi_\ell(\Delta)P_\ell \tag{10}$$

Both the quantities $\psi_\ell(\Delta)$ in (9) and $\psi_\ell(\Delta) - \beta(\Delta)$ in (10) are normalized according to

$$w = \begin{cases} 2\pi + w, & \text{if } w < -\pi, \\ w, & \text{if } |w| \le \pi, \\ 2\pi - w, & \text{if } w > \pi \end{cases} \tag{11}$$

In Table V, the statistical values of CAS for two scenarios are depicted. In the table, μ_A and σ_A are the parameters of the log-normal distributions when they are fitted to the CAS observations. In our measurement, the angle of departure (AOD) represents the angle radiated from BS and the angle of arrival (AOA) is used to describe the waves reached MS. The results in both scenarios show that at the same side, the CAS of NLOS case is nearly the same as that of LOS. In order to explain this result, one example of AOD and AOA in urban macro-BJ LOS case at 2.35GHz is given in Fig. 7. The star marks represent the arriving paths with the different angles and powers. The results indicate that even in LOS case, the rich reflections and scattering of BS and MS bring to a larger AS from the closely distributed buildings, numerous vehicles and other objects in surrounding environment. By contrast to urban macro-BJ at 2.35GHz, the CASs of AOA and AOD of micro-SJZ at 2.35GHz are slightly smaller. In urban macrocell, BS covers the larger area than that in microcell. So the MPCs possibly arrive at the Rx via reflection from remote scatterers, i.e. high buildings, etc. Thus it leads to a larger AS at urban macrocell. Such propagation environment characteristic results in our CASs of both AOA and AOD are larger than those of WINNER, i.e. the dense buildings and the obviously higher buildings, etc. The results given above indicate that we could explore the MIMO technique for IMT-Advanced system for the larger AS, which leads to the high system capacity [7].

IV. CONCLUSION

This paper presents the channel characteristics of 580MHz, 2.35GHz and 4.90GHz in the urban micro- and macrocell scenarios in the cities of China. Based on the extensive channel measurements, the empirical log-distance PL models are derived. In LOS case, all PL exponent n are a bit larger than 2. As for NLOS case, the exponent n of micro-SJZ is 3.7, which is slightly larger than those of macro-BJ and macro-SJZ. In LOS case, FDF C is equal to 19.8 and 32.1 for NLOS case by fitting the PL model of 2.35GHz and 4.90GHz. The statistic results show that a larger rms DS in urban microcell and

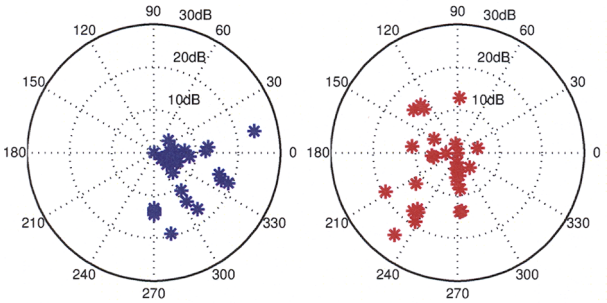

(a) AOD (b) AOA

Fig. 7. One example of AOD and AOA in urban macro-BJ LOS case at 2.35 GHz

TABLE V
STATISTICAL AZIMUTH CAS VALUES OF AOD AND AOA

Scenarios			Urban microcell		Urban macrocell	
			2.35GHz (SJZ)	WINNER [8]	2.35GHz (BJ)	WINNER [8]
CAS of AOD	LOS	Median [°]	18	N/A	17	N/A
		μ_A [$\log_{10}(°)$]	1.15	0.48	1.26	1.00
		σ_A [$\log_{10}(°)$]	0.49	0.37	0.31	0.25
	NLOS	Median [°]	17	N/A	28	N/A
		μ_A [$\log_{10}(°)$]	1.20	1.18	1.42	0.95
		σ_A [$\log_{10}(°)$]	0.39	0.21	0.28	0.22
CAS of AOA	LOS	Median [°]	66	N/A	71	N/A
		μ_A [$\log_{10}(°)$]	1.81	1.40	1.86	1.70
		σ_A [$\log_{10}(°)$]	0.18	0.20	0.27	0.19
	NLOS	Median [°]	64	N/A	66	N/A
		μ_A [$\log_{10}(°)$]	1.79	1.54	1.81	1.72
		σ_A [$\log_{10}(°)$]	0.16	0.20	0.24	0.14

AS of AOD and AOA are observed for the high density and height of buildings. As the frequency varying from 580MHz to 4.90GHz, the median rms DS is decreased from 110ns to 40ns for LOS case and from 330ns to 130ns for NLOS case. These results are necessary for the technical research and evaluation of IMT-Advanced system.

ACKNOWLEDGMENT

The authors would like to thank all members from BUPT and Elektrobit Corporation, Finland for their great efforts in the winter measurement campaigns. Useful help and suggestions from Dr. Xiongwen Zhao are greatly appreciated. Especially thanks to Research Institute of China Mobile to coordinate the measurement sites.

This work was supported in part by the National 863 High Technology Research and Development Program of China under Grant No. 2006AA01Z258, and by Research Institute of China Mobile.

REFERENCES

[1] ITU-R Document 8F/TEMP/568-E, "Working document towards proposed draft new [Report/Recommendation][Guidelines for Evaluation of Radio Interface Technologies for IMT-Advanced]," May 2007.

[2] ITU-R Rec. M.1225, "Guidelines for evaluation of radio transmission technologies (RTTs) for IMT-2000," 1997.

[3] Y. Oda, R. Tsuchihashi, K. Tsunekawa, and M. Hata, "Measured path loss and multipath propagation characteristics in UHF and microwave frequency bands for urban mobile communications," in *Proc. IEEE 53rd Vehicular Technology Conf. (VTC2001-Spring)*, vol. 1, 2001, pp. 337–341.

[4] T. Rautiainen, J. Juntunen, and K. Kalliola, "Propagation analysis at 5.3 GHz in typical and bad urban macrocellular environments," in *Proc. IEEE 65th Vehicular Technology Conf. (VTC2007-Spring)*, vol. 1, 2007, pp. 501–505.

[5] I. E. Telatar, "Capacity of multi-antenna Gaussian channels," *Europ. Trans. Telecommun.*, vol. 10, no. 6, pp. 585–595, Nov.–Dec. 1999.

[6] A. Goldsmith, S. Jafar, N. Jindal, and S. Vishwanath, "Capacity limits of MIMO channels," *IEEE J. Sel. Areas Commun.*, vol. 21, no. 5, pp. 684–702, Jun. 2003.

[7] H. Bolcskei, D. Gesbert, and A. Paulraj, "On the capacity of OFDM-based spatial multiplexing systems," *IEEE Trans. Commun.*, vol. 50, no. 2, pp. 225–234, Feb. 2002.

[8] "IST-4-027756 WINNER II D1.1.2 V1.0 WINNER II channel models," Sep. 2007. [Online]. Available: https://www.ist-winner.org/WINNER2-Deliverables/D1.1.2.pdf

[9] V. Jungnickel, S. Jaeckel, L. Thiele, U. Krueger, A. Brylka, and C. von Helmolt, "Capacity measurements in a multicell MIMO system," in *Proc. IEEE Global Telecommunications Conference (GLOBECOM '06)*, Nov. 2006, pp. 1–6.

[10] X. Zhao, J. Kivinen, P. Vainikainen, and K. Skog, "Propagation characteristics for wideband outdoor mobile communications at 5.3 GHz," *IEEE J. Sel. Areas Commun.*, vol. 20, no. 3, pp. 507–514, Apr. 2002.

[11] J. Zhang, X. Gao, P. Zhang, and X. Yin, "Propagation characteristics of wideband MIMO channel in hotspot areas at 5.25 GHZ," in *Proc. IEEE 18th International Symposium on Personal, Indoor and Mobile Radio Communications (PIMRC 2007)*, Sep. 2007, pp. 1–5.

[12] J. J. Park, W. S. Kim, M. D. Kim, and H. K. Chung, "Measurement results at 3.7 GHz in urban macrocell environment," in *Proc. IEEE 66th Vehicular Technology Conf. (VTC2007-Fall)*, 2007, pp. 864–868.

[13] Y. Ohta and T. Fujii, "Delay profile prediction in microwave-band for wideband radio propagation," in *Proc. 2005 International Symposium on Antennas and Propagation (ISAP2005)*, vol. 3, Seoul, 2005, pp. 1105–1108.

[14] B. Fleury, M. Tschudin, R. Heddergott, D. Dahlhaus, and K. Ingeman Pedersen, "Channel parameter estimation in mobile radio environments using the SAGE algorithm," *IEEE J. Sel. Areas Commun.*, vol. 17, no. 3, pp. 434–450, Mar. 1999.

[15] "Propsound multidimensional channel sounder." [Online]. Available: http://www.propsim.com

[16] V. Erceg, L. Greenstein, S. Tjandra, S. Parkoff, A. Gupta, B. Kulic, A. Julius, and R. Bianchi, "An empirically based path loss model for wireless channels in suburban environments," *IEEE J. Sel. Areas Commun.*, vol. 17, no. 7, pp. 1205–1211, 1999.

[17] T. S. Rappaport, *Wireless Communications: Principles and Practice*, 2nd ed. Prentice Hall PTR, 2002.

[18] M. Hata, "Empirical formula for propagation loss in land mobile radio services," *IEEE Trans. Veh. Technol.*, vol. 29, no. 3, pp. 317–325, 1980.

[19] COST Action 231, *Digital mobile radio towards future generation systems*. European Commission, 1999.

[20] P. Papazian, "Basic transmission loss and delay spread measurements for frequencies between 430 and 5750 MHz," *IEEE Trans. Antennas Propag.*, vol. 53, no. 2, pp. 694–701, 2005.